Journal of Biomolecular Structure & Dynamics, ISSN 0739-1102
Volume 23, Issue Number 4, (2006)

Cation-Mediated Interplay of Loops in Chaperonin-10

http://www.jbsdonline.com

Swetha Vijayakrishnan[1]
Rohini Qamra[2]
Chandra S. Verma[3,4,*]
Ranjan Sen[1,*]
Shekhar C. Mande[1,*]

[1]Centre for DNA Fingerprinting and Diagnostics
ECIL Road, Nacharam
Hyderabad 500 076 India
[2]Department of Biophysics
University of Delhi, South Campus
Benito Juarez Road
New Delhi 110021 India
[3]Structural Biology Laboratory
Department of Chemistry
University of York
YORK YO10 5YW
[4]Bioinformatics Institute
30 Biopolis Way
#07-01 MATRIX
Singapore 138671

Phone: +91-40-27171442
Fax: +91-40-27155610
Email: shekhar@cdfd.org.in
Email: rsen@cdfd.org.in
Email: chandra@bii.a-star.edu.sg

Abstract

The ubiquitously occurring chaperonins consist of a large tetradecameric Chaperonin-60, forming a cylindrical assembly, and a smaller heptameric Chaperonin-10. For a functional protein folding cycle, Chaperonin-10 caps the cylindrical Chaperonin-60 from one end forming an asymmetric complex. The oligomeric assembly of Chaperonin-10 is known to be highly plastic in nature. In *Mycobacterium tuberculosis*, the plasticity has been shown to be modulated by reversible binding of divalent cations. Binding of cations confers rigidity to the metal binding loop, and also promotes stability of the oligomeric structure. We have probed the conformational effects of cation binding on the Chaperonin-10 structure through fluorescence studies and molecular dynamics simulations. Fluorescence studies show that cation binding induces reduced exposure and flexibility of the dome loop. The simulations corroborate these results and further indicate a complex landscape of correlated motions between different parts of the molecule. They also show a fascinating interplay between two distantly spaced loops, the metal binding "dome loop" and the GroEL-binding "mobile loop", suggesting an important cation-mediated role in the recognition of Chaperonin-60. In the presence of cations the mobile loop appears poised to dock onto the Chaperonin-60 structure. The divalent metal ions may thus act as key elements in the protein folding cycle, and trigger a conformational switch for molecular recognition.

Introduction

Chaperonins are among the best characterized classes of molecular chaperones and are known to occur ubiquitously in bacteria as well as in eukaryotes. The two members of this class, Chaperonin-60 (Cpn-60) and Chaperonin-10 (Cpn-10), have served as a paradigm for chaperone mediated protein folding with numerous studies resulting in an intricate mechanism for this process (1-3). It has been observed that protein folding *in vivo* occurs in the larger cavity of the Cpn-60 cylinder where unfolded or partially folded peptides are sequestered. Release and binding of polypeptides from Cpn-60 surfaces is tightly regulated by Cpn-10. Binding of ATP and a Cpn-10 heptamer to the *cis* ring of a Cpn-60 tetradecamer results in an enlargement of the hydrophilic central cavity, which sequesters the polypeptides and provides a conducive environment to fold (4). ATP hydrolysis in the *cis* ring, accompanied by ATP binding in the *trans* ring, promotes Cpn-10 dissociation from the complex and release of the substrate polypeptide from the central cavity (5).

Crystal structures of *E. coli* Cpn-10 (6) as well as its homologues from *Mycobacterium leprae* (7), *Mycobacterium tuberculosis* (8, 9) and *Thermus thermophilus* (10) are known to atomic resolutions. Cpn-10 forms a single heptameric ring of identical subunits of 10 kDa each. The overall structure of Cpn-10 resembles a dome with an orifice of 8-12 Å diameter. The Cpn-10 heptamer can cap either to one end or both ends of Cpn-60 resulting in an asymmetric or a symmetric complex, respectively. The *M. tuberculosis* Cpn-10 (*Mt* Cpn-10) monomer consists of 99 residues forming a conserved hydrophobic β-barrel core, with β-strands of the barrel connected by β-hairpins. The hairpin comprising residues 48 to 58

and extending from the top of the dome, called the "dome loop" (11) is highly negatively charged at its tip and is partially stabilized in the presence of metal ions. The other hairpin comprising residues 18 to 38 and extending down the dome, called the "mobile loop" (11, 12), is responsible for specific binding of Cpn-10 to Cpn-60 (Fig. 1). There is also a third small flexible loop comprising residues 76 to 88 that we choose to call as the "hind loop" (Fig. 1). This hind loop is thought to play a key role in facilitating conformational changes in the mobile loop and thereby efficient binding of Cpn-10 to Cpn-60 (13).

The tip of the dome is also the closest approach to the seven-fold symmetry axis in the *Mt* Cpn-10, where three acidic residues, D51, E52, and D53, are located (Fig. 1). The conglomeration of acidic residues, therefore, results in a very high negative potential towards the top of the *Mt* Cpn-10 dome (13, 14). The repulsive electrostatic forces thereby lead to an altered flexibility of the dome and possibly the instability of the oligomeric assembly (14). It is significant to note that Cpn-10 of *E. coli* has previously been proposed to have a metastable oligomeric structure leading to an increase in the diameter of the dome orifice in solution (15). The evolutionary conservation of flanking residues (residue positions 46-48 preceding the dome loop and residue positions 65 and 66 following the loop) and the charged residues at the tip of the loop (residue positions 51-53) suggest a possible critical role of the dome loop in the *Mt* Cpn-10 function (14). It has recently been shown that metal ion binding to the dome loop modulates the different plastic states of *Mt* Cpn-10 and enhances the stability of the oligomeric structure. It has also been proposed that the utilization of negative charges on the surface of the dome and their neutralization with metal ions enables the flexible dome loop to act as a "Conformational Switch" for the Cpn-10-Cpn-60 interaction (14). In this work, we have explored the consequence of metal ion-binding at the dome loop, and whether the conformational changes in the dome loop due to metal-binding are effectively transmitted to different parts of the *Mt* Cpn-10 structure.

There have been several illuminating computational studies probing the dynamics of the Cpn-10-Cpn-60 complex (16-18), however, there has been no work reported to date examining the dynamics of Cpn-10 alone. Additionally, there is relatively little work done on the effects of metal ions on the dynamics/flexibility of proteins (19, 20). In the present study, we have carried out fluorescence experiments to probe the flexibility of the metal-binding regions of *Mt* Cpn-10 followed by molecular dynamics (MD) simulations of the protein. The MD simulations were carried out in an attempt to gain atomic level insights into the influence of the metal ion upon the conformational changes in the protein.

Materials and Methods

Generation of the Dome Loop Mutant and Purification

The *Mt* Cpn-10 mutant, with the three acidic residues at the dome replaced by valine or alanine, was constructed using the Quik-Change site-directed mutagenesis kit (Stratagene). The forward and reverse primers for mutagenesis of D51V, E52A, and D53V were 5′-GGCCGGTGGGTCGCGGTCGGCGAGAAGCGG-3′ and 5′-CCGCTTCTCGCCGACCGCGACCCACCGGCC-3′, respectively, with the underlined nucleotides denoting the changed residues. Purification of the wild type and mutant protein was performed as previously described (14).

Assessment of Ca^{2+} Binding

Fluorescence emission of tryptophan as a function of changing Ca^{2+} ion concentration (100nM to 10mM) was used as a probe for conformational changes through equilibrium binding studies. The reaction mixtures containing 2μM (protomer) Cpn-10 in 10mM Tris-Cl, pH 8.0 were incubated with Ca^{2+} in a total reaction vol-

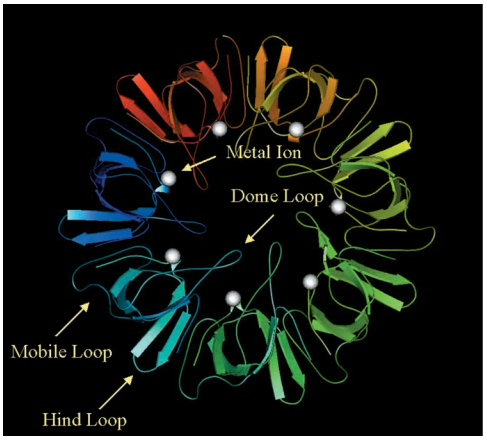

Figure 1: View of the crystal structure of the *M. tuberculosis* Cpn-10 with metal ions. The ribbon diagram was drawn with MOLSCRIPT (36). Each subunit is shown in a different color and the metal ions are colored in white. The loop regions have been marked accordingly.

ume of 200µl at 25 °C. The excitation wavelength was set at 295 nm and emission was measured in the range 310 and 500 nm. The equilibrium binding constant for the wild type Cpn-10 was determined by the increase in fluorescence upon ligand binding. Steady-state emission at each ligand concentration was monitored at 340nm and the observed fluorescence intensity corrected for the emission intensity of the reference buffer. Apparent binding constant (K_{app}) was determined by means of the following Equation [1] (21):

$$1/\Delta F = 1/\Delta F_{max} + 1/[K_{app} \cdot F_{max}(c_p - c_o)] \quad [1]$$

where ΔF is the change in fluorescence emission intensity at 340 nm (λ_{ex} = 295 nm) upon addition of different concentrations of Ca^{2+} and ΔF_{max} is the same parameter when the ligand is totally bound to the protein. c_p is the concentration of the protein and c_o is the initial concentration of the ligand. This equation is valid when $c_o >> c_p$. A linear plot of $1/\Delta F$ against $1/(c_p - c_o)$ was extrapolated to the ordinate. The reciprocal of the intercept on the ordinate gave the value of ΔF_{max}. K_{app} was obtained from the ratio of the intercept and the slope of the plot.

Fluorescence polarization anisotropy of the wild type and the dome loop mutant Cpn-10 was monitored at varying concentrations of Ca^{2+}. 2µM Cpn-10 in 10mM Tris-Cl, pH 8.0 was incubated with Ca^{2+}, with concentrations of Ca^{2+} varying from 100nM to 10mM. Parallel and perpendicular emission components were measured by excitation at 295nm with a 5.5nm slit width. Emission was monitored through 8nm slit width at 340nm. In each anisotropy measurement, the parallel and perpendicular intensity of the background buffer solutions were subtracted from the measured values of the sample and the anisotropy was calculated. Measurements were repeated three times at each titration point and the resulting anisotropy values were averaged.

Fluorescence quenching experiments were performed with acrylamide as an external quencher. Acrylamide was added from a 1M stock solution to a final concentration ranging from 0.01M to 0.1M. Quenching was performed in the absence or presence of 1mM Ca^{2+} added to 2µM wild-type Cpn-10 in 100mM Tris-Cl, pH 8.0 at 25 °C. The data were corrected for the dilution introduced by the addition of acrylamide. The fluorescence quenching data were analyzed according to the Stern-Volmer relationship [2] (22):

$$Fo/F = 1 + K_{SV}[Q] \quad [2]$$

where Fo and F are the fluorescence intensities in the absence and presence of acrylamide, respectively. [Q] is the acrylamide concentration and K_{SV} is the quenching constant. The fraction of accessibility (fe) of the tryptophan residue was calculated from the Equation [3] (23, 24):

$$Fo/(Fo-F) = 1/(K_{SV} f_e[Q]) + 1/f_e \quad [3]$$

Molecular Dynamics Simulations

Two MD simulations were carried out, one in the presence of calcium ions and the other in its absence (henceforth referred to as ION and NOION, respectively). The X-ray crystal structure of *Mt* Cpn-10 (8) (PDB code-1HX5) was taken as the starting structure for the study. Each monomer in the crystal structure has 97 amino acids with density for residues 1-4, 17-21, 31-36, and 98-99 missing. Hence, the numbering system used in our work will be from 1-93 in the subsequent text, with residues 1 and 93 corresponding to residues 5 and 97 in the crystal structure, respectively. While the terminal missing residues were left out, residues 17-21 and 31-36 were modeled on a monomer and the heptamer was generated accordingly. The models were constructed based upon the coordinates of the GroES:GroEL complex of *E. coli* (PDB code-1AON) (4). Ca^{2+} ions were modeled into each monomer on the basis of the position of the divalent ions observed in the crystal structure of *Mt* Cpn-10 (8). Ions were modeled in such a manner that each ion was stabilized by residues E9 and W50 of one monomer, and D61 of the neighboring subunit (residues 5, 46, and 57 in the renumbered system). The ions were placed at the positions of highest electronegativity, which roughly corresponded to the centre of the coordinates of the charged oxygens of the three residues. The ions were constrained during minimization but were free to move during the part of the simulations that was used for analysis.

The system was explicitly solvated with a shell of TIP3 water molecules (25) using the MOIL-View (26) program in the AMBER software suite. The number of TIP3 water molecules added to the system was 8735. Non-bonded electrostatic interactions, scaled by a constant dielectric value of 1.0, were shifted to zero at 12Å while a switching function was used to truncate the van der Waals interactions between 8-12Å; non-bonded lists were generated over 14Å. The simulations were carried out using the program CHARMM and its associated force field (27, 28). The conformation of the solvated protein system was first relaxed *via* a series of energy minimizations under harmonic constraints that were periodically reduced until zero. This was followed by MD simulations at 300K where the bonds to hydrogens were constrained using SHAKE (29) with a relative tolerance of 1.0×10^{-6}. The Leap Frog algorithm was used to calculate the Newton's laws at time intervals of 1fs for a total of 2ns. Coordinates were saved every 1ps. The last 1.8ns of each simulation was used for analysis. The tools used for analyses included GROMACS (30, 31), VMD (32), SQUID (33), GRASP (34), Swiss PDB Viewer (35), MOLSCRIPT (36), and other locally written codes.

Results and Discussion

The plasticity of *Mt* Cpn-10 has been shown to arise due to the accumulation of acidic residues at the tip of the dome loop (Fig. 1). Moreover, addition of divalent cations has been shown to be effective in neutralizing the negative charges at the dome loop (14). In order to assess if the negative charges and the oligomeric plasticity were indeed correlated, a *Mt* Cpn-10 mutant, where the three acidic residues were replaced by valine or alanine, was constructed. Sequencing of the mutant gene confirmed that the mutant protein contained V, A, and V in place of D51, E52, and D53, respectively.

Conformational Changes Effected by Ca2+

The only tryptophan residue in the *Mt* Cpn-10 is present in the dome loop and lies at the monomer-monomer interface thereby serving as a probe for micro-conformational changes that occur upon ligand binding. In order to investigate interactions between Ca^{2+} and *Mt* Cpn-10, equilibrium binding was assessed through fluorescence intensity changes. As shown in Figure 2A, the emission intensity increased with increasing Ca^{2+} ion concentrations till it reached a saturation value

at a concentration of 1mM in the wild type Cpn-10. The apparent binding constant thus calculated was $0.007\mu M^{-1}$ (dissociation constant, K_d = 143μM) indicating a strong interaction between Ca^{2+} and the wild type Cpn-10. However, in contrast to the wild type, the emission intensity of the dome loop mutant upon variation of Ca^{2+} ion concentration remained relatively constant (Fig. 2B), thus suggesting that the mutant protein might not bind Ca^{2+}.

Fluorescence anisotropy measurements provide a powerful means of assessing conformational changes, especially in cases like *Mt* Cpn-10, where the observations are due to a single tryptophan residue. Solvent exposure of W50 (W46 in the renumbered sequence) was measured through fluorescence anisotropy, which was thus exploited to probe conformational changes as a result of Ca^{2+} binding to the dome loop. Fluorescence anisotropy of tryptophan resulted in a profile as shown in Figure 2C. Binding of Ca^{2+} to the wild type *Mt* Cpn-10 resulted in a steady increase in fluorescence anisotropy indicating a decrease in the rotational freedom of the tryptophan, till saturation was achieved at 1mM. The dome loop mutant on the other hand did not exhibit any alteration in fluorescence anisotropy, corroborating our earlier data that the mutant does not exhibit Ca^{2+} dependent conformational changes. Thus, the dome loop mutant might have an impaired Ca^{2+} binding ability.

The fluorescence data thus clearly indicate that the ability of *Mt* Cpn-10 to bind Ca^{2+} ions is a consequence of the negative charges at the tip of the dome loop. Since Ca^{2+} binding is known to bring about a reduced plasticity to the heptameric molecule, it was apparent that binding by divalent cations would result in conformational changes in the dome loop.

In order to assess these conformational changes in *Mt* Cpn-10, fluorescence quenching experiments with acrylamide were performed for the wild type protein in the absence and presence of Ca^{2+}. Since the dome loop mutant did not exhibit any change in fluorescence intensity upon addition of Ca^{2+} it was not used for quenching studies. The K_{SV} constant for acrylamide quenching of Cpn-10, obtained from the Stern-Volmer plot was $9.9M^{-1}$ in the presence of Ca^{2+}. Interestingly, K_{SV} in the absence of Ca^{2+} was much higher, with a value of $17.5M^{-1}$. A decrease in K_{SV} in the presence of Ca^{2+} suggests that upon Ca^{2+} binding, the tryptophan becomes less exposed in comparison to that during the absence of Ca^{2+} ions. Moreover, the fractional accessibility of the tryptophans in the presence of Ca^{2+} was 0.08 in comparison to 0.35 in the absence of the divalent cation. A decrease in K_{SV} in the presence of Ca^{2+} and also a reduced fractional accessibility suggests that upon Ca^{2+} binding, the tryptophans becomes less exposed in comparison to that during the absence of Ca^{2+} ions. This corroborates with a previous report where addition of divalent cations was shown to promote burial of W50 (W46 in the renumbered sequence) (14). It is pertinent to note that since the negative charges and

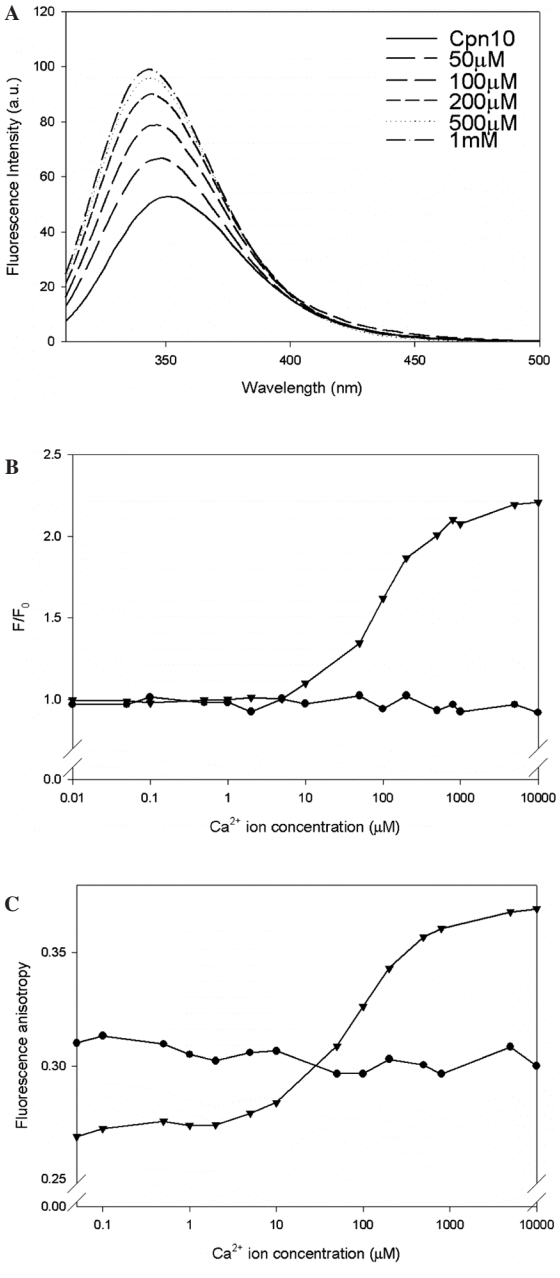

Figure 2: Effect of Ca^{2+} concentration of changes in fluorescence. The reaction mixtures containing 2μM (protomer) Cpn-10 in 10mM Tris-Cl, pH 8.0 were incubated with Ca^{2+} in a total reaction volume of 200μl at 25 °C. The excitation wavelength was set at 295 nm and emission was measured in the range 310 and 500 nm on a Perkin Elmer LS55 spectrofluorimeter. (**A**) The intensity of fluorescence showed steady increase till the concentration of Ca^{2+} reached 1mM. Concomitant with the increase in intensity, there was also a blue shift in λ_{max}. Concentrations in the figure indicate that of Ca^{2+} (**B**) Fluorescence intensity at 340 nm showed steady increase in the wild type (▼) with increasing concentration of Ca^{2+} ions compared with that in the dome loop mutant (●), indicating that the mutant has impaired Ca^{2+} binding. (**C**) Effect of Ca^{2+} binding on fluorescence anisotropy was measured as a function of Ca^{2+} ion concentration. 2μM Cpn-10 was incubated with Ca^{2+}, with concentrations varying from 100nM to 10mM. Parallel and perpendicular emission components were measured by excitation at 295nm with a 5.5nm slit width. Emission was monitored through 8nm slit width at 340nm. (▼) denote anisotropy for the wild type protein, while (●) denote that for the dome loop mutant. It is clear that the anisotropy for the dome mutant remains unaltered, suggesting that Ca^{2+} ions do not affect the conformation of the dome loop.

Figure 3: RMSFs of the Cα coordinates from their time-averaged values as a function of residue numbers. Panels (**A**) to (**G**) indicate the RMSFs for the seven different subunits of *Mt* Cpn-10. The highly flexible loop regions are indicated by vertical arrows and labeled as ML: mobile loop (residues 14-32), DL: dome loop (residues 43-54), and HL: hind loop (residues 72-84). These three regions consistently show high RMSF values in all the subunits. Position of Trp46 is also marked.

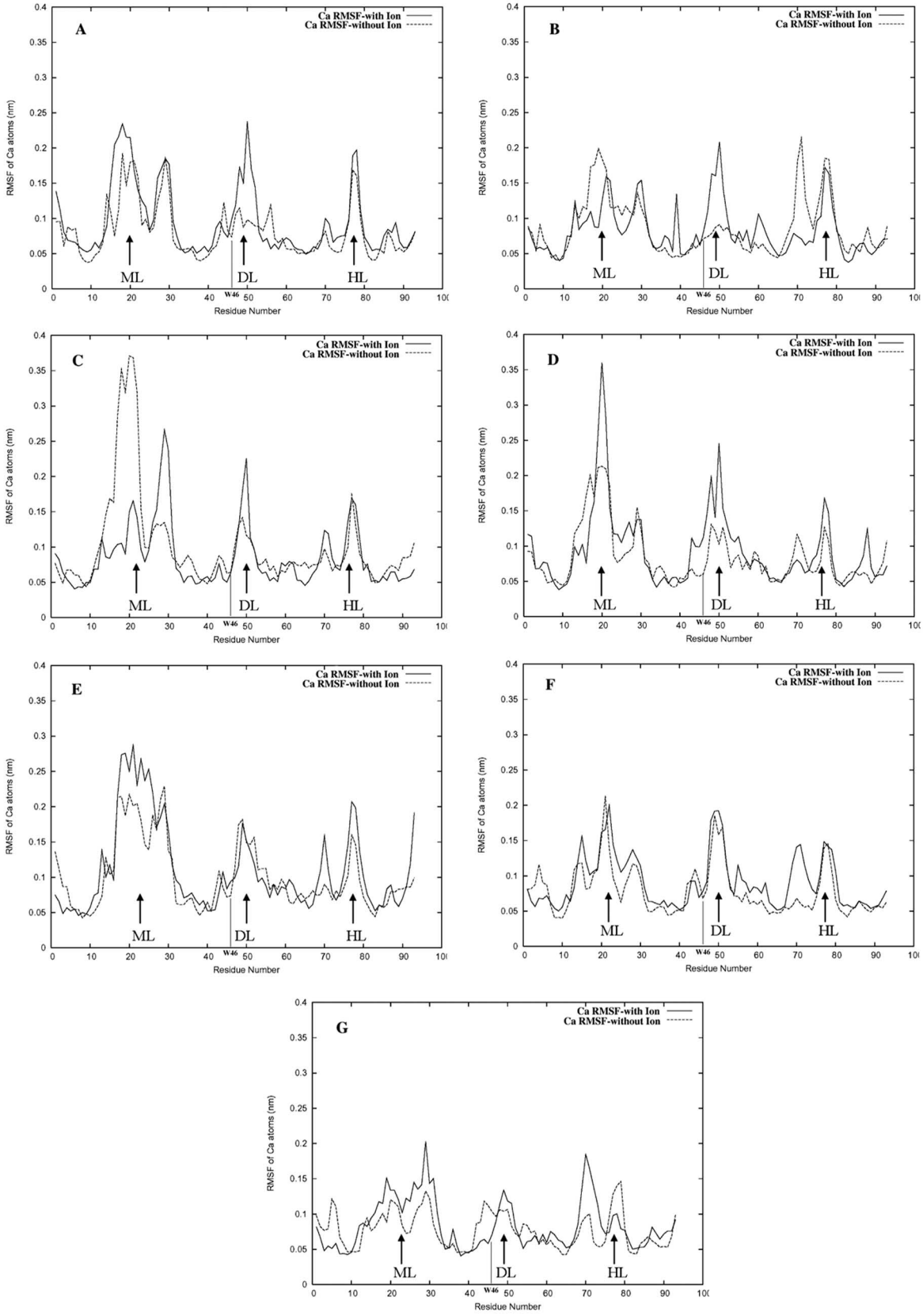

also the flanking residues at the dome are known to be evolutionarily conserved, binding by divalent cations and hence the conformational changes thereby induced at the dome, might have a relevance to the function of *Mt* Cpn-10.

Having shown that conformational changes indeed take place upon binding by divalent cations, it was interesting to probe how these changes are transmitted to the rest of the structure in order to bring reduced plasticity. Moreover, since large conformational changes in the mobile loop of Cpn-10s are known to occur during recognition by Cpn-60, it was also interesting to enquire if the two conformational changes were correlated. One of the means of investigating the transmittal of conformational changes was through molecular dynamics simulations. Differences in the simulations between those in the presence or in the absence of cations would reveal the atomic features of these conformational changes.

Flexibility of the Heptamer

Analysis of the temporal evolution of the root mean square deviation (RMSD) of the backbone atoms from the starting structure, with the mean values of 0.35nm in the presence of metal ion and 0.28nm in their absence, suggested that the simulation was stable (data not shown). Similarly temporal evolution of radius of gyration also suggested the same. Interestingly, during the course of simulation, the Ca^{2+} ions placed near the dome loop remained within interacting distance from the three crucial charged residues. Analysis of root mean square fluctuations (RMSF) across the sequence showed that the average fluctuations of the different monomers ranged from 0.06nm to 0.4nm in both ION and NOION. Moreover, a consistent pattern was seen across almost all the monomers (Fig. 3) whereby ION was characterized by higher flexibility (up to about 30%) in three regions: the dome loop, mobile loop, and the hind loop relative to the NOION system. This was further reflected by monitoring the flexibility of the backbone dihedral angles (using the MONITOR functionality of CHARMM): these were found to be larger in ION than in NOION (the number of backbone dihedral angles undergoing transitions being 7204 and 7063, respectively), again pointing to the enhanced flexibility of the system in the presence of metal ions. However, despite the overall higher flexibility in the dome loop observed in ION, locally a consistent decrease in the flexibility of the region including and immediately contiguous with W50 (W46 in the renumbered sequence) among all the monomers was observed (Fig. 3). As mentioned above, our fluorescence anisotropy and quenching data had suggested that addition of Ca^{2+} ions leads to reduced flexibility of the tryptophan. Thus, our MD data is in accord with the increased burial and reduced flexibility of tryptophan upon Ca^{2+} binding.

Variations in flexibility lead to correlated motions connecting spatially distant regions of proteins, a characteristic that is increasingly being recognized as an important player in modulating the structural and functional dynamics of proteins (16-18, 37, 38). This dynamic coupling between residues was examined by calculating the covariance between the fluctuations of the residues for ION and NOION (Fig. 4A and 4B). The extent of correlated motions exhibited by the heptamer was larger in ION. ION was also strikingly characterized by strong correlated couplings between neighboring monomers in groups of two or three, a feature that was reduced noticeably in NOION. In contrast, the NOION system was characterized by the appearance of anti-correlated motions spanning the whole system. The anti-correlated motions in ION were observed between subunits that are not contiguous suggesting that ION is characterized by very distinct anti-correlated motions across the orifice. These motions are similar to those that occur across binding-site clefts of enzymes and accompany ligand binding thereby suggesting that similar motions in Cpn-10 might be responsible for squeezing and releasing Cpn-60 (18, 39).

In order to examine the correlated motions in more detail the covariance matrix for monomer G, as a representative, was analyzed (Figs. 4C and 4D). The striking

observation was that strong correlations existed that coupled the hind loop to both the dome loop and the mobile loop in the presence of ions. Such motions were, however, much reduced in the absence of ions. The strong correlated motions in ION therefore suggested that the ion binding at the dome loop could be communicated to the mobile loop *via* subtle conformational changes.

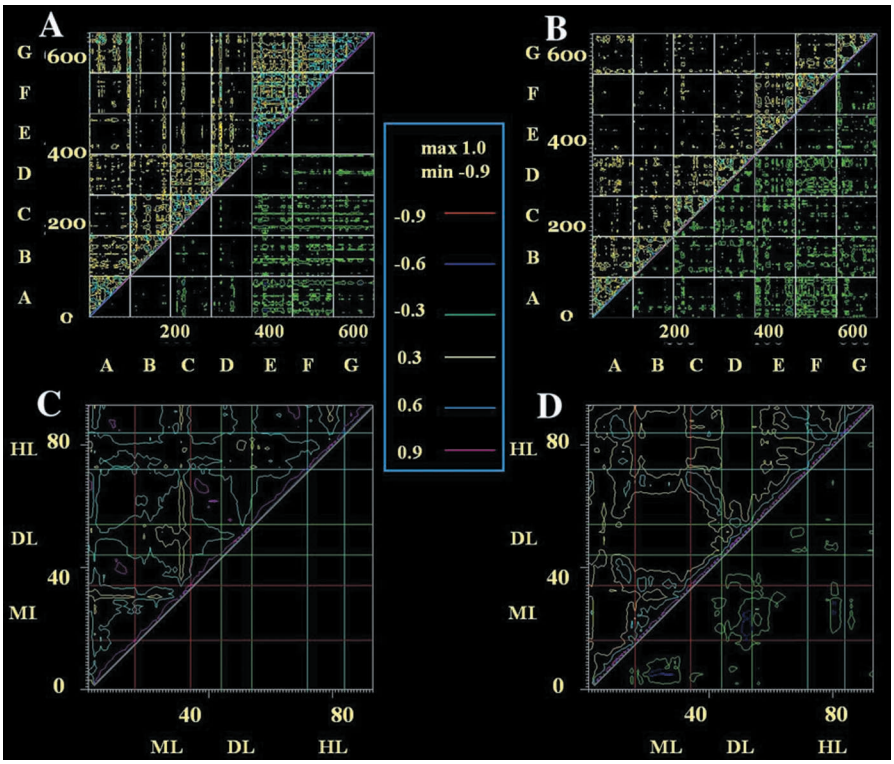

Figure 4: Matrix of covariance of the fluctuations of C^{α} atoms. Yellow, cyan, and pink regions indicate that the C^{α} atoms move in a concerted way (positively correlated movements), and blue, red, and green indicate that they move opposite to each other (anti-correlated movements). The scale is from -9 (red) to 9 (pink). In panels (**A**) (ION) and (**B**) (NOION), covariance of the whole heptamer is shown and the various subunits have been indicated by the alphabets A to G. In panels (**C**) (ION) and (**D**) (NOION) the covariance matrix for the fluctuations of the C^{α} atoms of the monomer G are shown. The loop regions in the monomer are delineated as ML (red lines), DL (green lines), and HL (cyan lines). All the maps were drawn using SQUID (33).

The overall differences in plasticity were also examined through the phase space dynamics of the system. Principal components (40) of the two trajectories showed that the conformational space sampled in ION was larger than in NOION (data not shown). A few of the lowest frequency components covered most of the fluctuations in both systems, however, the lowest frequency mode in ION had ~12% larger coverage of phase space. It was also obvious that the distribution became Gaussian in NOION more rapidly than in ION and was more multimodal in the latter, suggesting that the latter was characterized by greater complexity and therefore larger entropy.

Conformational Changes of the Loops

Mobile Loop: The Cpn-10 mobile loop has previously been shown to sample several conformations owing to its flexibility (41). The conformational space searched by the mobile loop of *Mt* Cpn-10 was analyzed by taking snapshots of the simulations taken every 100ps in the presence and absence of metal ions (data not shown). The conformational space searched was less restricted in the presence of metal ions. In addition, a downward movement of the loop was also apparent exclusively in ION.

Hind Loop: The conformational changes in mobile loop are brought about by a rigid body movement of the 72-84 stretch which we have coined the "hind loop" (13). Examination of the dot product of the vectors defining each of the two β-strands contiguous to this loop (data not shown) showed that they undergo a 5° decrease in the relative orientation between the two strands upon ion complexation. Thus, the sheet appeared to assume rigidity thereby acting as a local anchor. Local reduction in entropy coupled with enhanced flexibility has been reported for the Cpn-10-Cpn-60 system (18). Sequence conservation of the hind loop residues suggested that they might play a similar role in conferring partial stability to the mobile

loop in the Cpn-10 family (11). In addition, the 61-66 loop also showed interesting dynamics in the presence of the divalent metal ions.

Overall Effect of Ca^{2+} Binding on Mt Cpn-10 Structure

The Cpn-10-Cpn-60 complex has been shown to be responsible for the correct folding of various cellular proteins. Hence the recycling of this complex and dissociation of the substrate from the complex probably depends intimately on its dissociation. This implies that factors governing the affinity and interactions of Cpn-10 with Cpn-60 are of critical importance for efficient chaperonin function (18). Of these factors, a major driving force is the topology and flexibility of the interacting regions. It is this coupling that we examine in this study through comparative fluorescence analysis of metal binding and molecular dynamics simulations.

Fluorescence data and simulations suggest that metals play a crucial role in mediating conformational changes in Cpn-10. Polarisation anisotropy comparisons of the wild type and the dome loop mutant of Cpn-10 clearly indicate that parts of the dome loop in the mutant are more rigid than that in the wild type structure. These results therefore suggest that loss of the charged residues at the dome loop, or equivalently the addition of metal ions to the wild type protein, reduce the flexibility of the dome loop in Cpn-10. In addition, MD simulations reveal this part to be the region encompassing W50 (W46 in the renumbered sequence). Acrylamide quenching studies show that W50 (W46 in the renumbered sequence) in the wild type protein becomes less accessible in the presence of Ca^{2+}, suggesting the importance of metals in conferring stability to the dome loop. Interestingly, the MD simulations corroborated the results of fluorescence studies. Our results show that the inherent flexibility of *Mt* Cpn-10 is indeed modulated by the binding of metal ions.

One of the major characteristics underlying flexibility in macromolecules is the interaction between parts that are spatially distant, and indeed have a major role in influencing function (16-18). In Cpn-10 the mobile loop is known to undergo a "folding-transition" from a disordered to an ordered state upon complexation with Cpn-60 (42) and might be assisted by the hind loop (13). The enhanced flexibility in the presence of ions could be a mechanism to assist this transition by lowering the barriers in the phase space for this conformational change (39). Our correlation plots reveal a significant increase in the correlated motions of the heptamer as well as each monomer in the presence of ions. Increased correlated motions in the presence of metal suggests that Cpn-10 may have acquired dominance of motions like breathing modes, which may be necessary for it to bind to Cpn-60 in order to carry out its efficient folding and allosteric functions. The development of correlated motions between blocks of monomers (18) and anti-correlations across the orifice are particularly strong in the presence of metal. The tight coupling between loops suggests that metal ions may assist in the transmission of signals across the molecule.

As the Cpn-10-Cpn-60 ternary complex serves as a powerful folding machine, the chemical and physical nature of its cavity influences the efficiency and specificity of the folding mechanism. Our data and observations lead us to the following two alternative mechanisms for the metal assisted functioning of Cpn-10:

I. The metal ions remain bound and induce breathing motions in the molecule, thereby facilitating folding of the trapped substrate within the Cpn-60 cavity. This breathing motion may result in exposure of more hydrophobic residues when the ring expands and the clustering of more hydrophilic residues when it shrinks. Such a motion would be of great importance for effective protein folding. It is also probable that while some substrates prefer a hydrophilic environment, there may be others that fold *via* transient intermediates and are more stabilized in hydrophobic environments. Thus binding of divalent ions may serve as

a way of fine-tuning the exposure of hydrophobic residues for binding of unfolded substrate peptides (43).

II. The metal ions only facilitate the complex formation of Cpn-60 and Cpn-10, without actively participating in the protein folding cycle. Once the Cpn-10-Cpn-60 complex is formed, the metal ions may be ejected out and the complex may resume its chaperone function. Thus the presence of metal ions may be transient and instrumental in initiating complex formation.

Besides the fundamental interest in the effects of metal ions on protein stability, the work is also of importance as the *Mt* Cpn-10 molecule has been implicated as a possible biomarker in tuberculosis (44, 45), and in bone remodeling in Pott's disease, a pathology resulting from tuberculosis (46). The latter becomes even more meaningful as bone remodeling involves calcium, which incidentally, is the metal ion in our study. In the models created by Meghji *et al*. (46), two regions, the mobile loop and the 61-66 loop region were experimentally observed to be linked to bone resorption and yet were found to be too buried to be accessible to antibodies. In our present study, we find that the 61-66 loop region is accessible (~109 $Å^2$) and this accessibility is somewhat enhanced by calcium (data not shown). On the other hand, the mobile loop region is quite exposed and its mobility is enhanced significantly by calcium. This could provide a means of controlling the flexibility of this loop with metal ions and providing a dynamic template for raising therapeutic antibodies against this epitope in an effort to control bone disease associated with vertebral tuberculosis.

In conclusion, fluorescence studies corroborated with molecular dynamics simulations suggested that Ca^{2+} ions effect conformational changes in *Mt* Cpn-10 structure. The motions of the three flexible loops in the structure appeared to be correlated, especially in the presence of metal ions. Thus, the metal ions might impart crucial functional properties to the protein. Metal ions might induce breathing motions in *Mt* Cpn-10 thereby leading to subtle exposure of hydrophobic regions important for the protein folding process. Alternatively, metal ions might just facilitate the complex formation between Cpn-10 and Cpn-60.

Acknowledgements

Our thanks to the Bioinformatics facility at CDFD, Hyderabad, for providing access to computer time. We are grateful to S. E. Hasnain for overall support. We thank the Royal Society, UK for the travel grant to C. V. Financial support from the Department of Biotechnology and The Wellcome Trust, UK is gratefully acknowledged. R. S. and S. C. M. are The Wellcome Trust International Senior Research Fellows.

References and Footnotes

1. F. U. Hartl. *Nature 381*, 571-580 (1996).
2. W. A. Fenton and A. L. Horwich. *Prot. Sci. 6*, 743-760 (1997).
3. P. B. Sigler, Z. Xu, H. S. Rye, S. G. Burston, W. A. Fenton, and A. L., Horwich. *Annu. Rev. Biochem. 67*, 581-608 (1998).
4. Z. Xu, A. L. Horwich, and P. B. Sigler. *Nature 388*, 741-750 (1997).
5. H. S. Rye, S. G. Burston, W. A. Fenton, J. M. Beecham, Z. Xu, P. B. Sigler, and A. L. Horwich. *Nature 388*, 792-798 (1997).
6. J. F. Hunt, A. J. Weaver, S. J. Landry, L. Gierasch, and J. Deisenhofer. *Nature 379*, 37-45 (1996).
7. S. C. Mande, V. Mehra, B. R. Bloom, and W. G. J. Hol. *Science 271*, 203-207 (1996).
8. B. Taneja and S. C. Mande. *Acta. Cryst. D. 58*, 260-266 (2002).
9. M. M. Roberts, A. R. Coker, G. Fossati, P. Mascagni, A. R. M. Coates, and S. P. Wood. *J. Bact. 185*, 4172-4185 (2003).
10. N. Numoto, A. Kita, and K. Miki. *Proteins 58*, 498-500 (2005).
11. B. Taneja and S. C. Mande. *Prot. Engg. 12*, 815-818 (1999).
12. S. J. Landry, J. Zeilstra-Ryalls, O. Fayet, C. Georgopoulos, and L. M. Gierasch. *Nature 364*, 255-258 (1993).
13. B. Taneja and S. C. Mande. *Curr. Sci. 81*, 87-91 (2001).

14. B. Taneja and S. C. Mande. *Prot. Engg. 14*, 391-395 (2001).
15. A. A. Timchenko, B. S. Melnik, H. Kihara, K. Kimura, and G. V. Semisotnov. *FEBS Lett. 471*, 211-214 (2000).
16. J. Ma and M. Karplus. *Proc. Natl. Acad. Sci. USA 95*, 8502-8507 (1998).
17. B. L. de Groot, H. J. C. Berendsen, and G. Vriend. *J. Mol. Biol. 286*, 1241-1249 (1999).
18. O. Keskin, I. Bahar, D. Flatow, D. G. Covell, and R. L. Jernigan. *Biochem. 41*, 491-501 (2002).
19. A. B. M. Linssen. *Ph.D. Thesis*, pp, 140. University of Groningen, Netherlands (1998).
20. G. Zoldak, M. Sprinzl, and E. Sedlak. *Eur. J. Biochem. 271*, 48-57 (2004).
21. J. L. Wang and G. M. Edelman. *J. Biol. Chem. 246*, 1185-1191 (1971).
22. S. S. Lehrer. *Biochemistry 10*, 3254-3263 (1971).
23. S. S. Lehrer and P. C. Leavis. *Meth. Enzymol. 49*, 222-236 (1978).
24. M. R. Eftink and C. A. Ghiron. *Anal. Biochem. 114*, 199-227 (1981).
25. W. L. Jorgensen, J. Chandrasekhar, J. D. Madura, R. W. Impey, and M. L. Klein. *J. Chem. Phys. 79*, 926-935 (1983).
26. C. Simmerling, R. Elber, and J. Zhang. In *Modeling of Biomolecular Structure and Mechanisms*, pp. 241-265. Eds., J. Pullman, *et al*. Kluwer, Netherlands (1995).
27. B. R. Brooks, R. E. Bruccoleri, B. D. Olafson, D. J. States, S. Swaminathan, and M. Karplus. *J. Comp. Chem. 4*, 187-217 (1983).
28. A. D. MacKerell, Jr., D. Bashford, M. Bellott, R. L. Dunbrack, Jr., J. D. Evanseck, M. J. Field, S. Fischer, J. Gao, H. Guo, S. Ha, D. Joseph-McCarthy, L. Kuchnir, K. Kuczera, F. T. K. Lau, C. Mattos, S. Michnick, T. Ngo, D. T. Nguyen, B. Prodhom, W. E. Reiher, III, B. Roux, M. Schlenkrich, J. C. Smith, R. Stote, J. Straub, M. Watanabe, J. Wiorkiewicz-Kuczera, D. Yin, and M. Karplus. *J. Phys. Chem. B. 102*, 3586-3616 (1998).
29. J. P. Ryckaert, G. Ciccotti, and H. J. C. Berendsen. *J. Comp. Phys. 23*, 327-341 (1977).
30. H. J. C. Berendsen, D. van der Spoel, and R. van Drunen. *Comp. Phys. Commun. 91*, 43-56 (1995).
31. E. Lindahl, B. Hess, and D. van der Spoel. *J. Mol. Mod. 7*, 306-317 (2001).
32. W. Humphrey, A. Dalke, and K. Schulten. *J. Molec. Graph. 14*, 33-38 (1996).
33. T. Oldfield. *J. Mol. Graph. 10*, 247-252 (1992).
34. A. Nicholls, K. Sharp, and B. Honig. *Prot. Struct. Funct. Genet. 11*, 281-296 (1991).
35. N. Guex and M. C. Peitsch. *Electrophoresis. 18*, 2714-2723 (1997).
36. P. J. Kraulis. *J. Appl. Crystallogr. 24*, 946-950 (1991).
37. J. L. Radkiewicz and C. L. Brooks, III. *J. Am. Chem. Soc. 122*, 225-231 (2000).
38. J. L. Radkiewicz, T. H. Rod, and C. L. Brooks, III. *Proc. Natl. Acad. Sci. USA. 100*, 6980-6985 (2003).
39. R. Dvorsky, J. Sevcik, L. S. D. Caves, and C. S. Verma. *J. Phys. Chem. B. 104*, 10387-10397 (2000).
40. S. Hayward and N. Go. *Ann. Rev. Phys. Chem. 46*, 223-250 (1995).
41. S. J. Landry, A. Taher, C. Georgopoulos, and S. M. van der Vies. *Proc. Natl. Acad. Sci. USA 93*, 11622-11627 (1996).
42. F. Shewmaker, K. Maskos, C. Simmerling, and S. J. Landry. *J. Biol. Chem. 276*, 31257-31264 (2001).
43. M. R. Betancourt and D. Thirumalai. *J. Mol. Biol. 287*, 627-644 (1999).
44. B. Chua-Intra, R. J. Wilkinson, and J. Ivanyi. *Infect. Immun. 70*, 1645-1647 (2002).
45. R. Hussain, F. Shahid, S. Zafar, M. Dojki, and H. M. Dockrell. *Immunology. 111*, 462-471 (2004).
46. S. Meghji, P. A. White, S. P. Nair, K. Reddi, K. Heron, B. Henderson, A. Zaliani, G. Fossati, P. Mascagni, J. F. Hunt, M. M. Roberts, and A. R. Coates. *J. Exp. Med. 186*, 1241-1246 (1997).

Date Received: August 3, 2005

Communicated by the Editor Manju Bansal